World Journal of Advanced Research and Reviews, 2020, 08(02), 131–140

World Journal of Advanced Research and Reviews

e-ISSN: 2581-9615, Cross Ref DOI: 10.30574/wjarr

Journal homepage: https://www.wjarr.com

(RESEARCH ARTICLE)

Ab initio structure determination and morphology study of $La_{1.26}\,Zr_{0.25}\,Na_{2.5}\,N_{0.24}\,O_{2.54}$ triclinic structure from powder x-ray diffraction data.

Bimal K Kanth and Parashuram Mishra*

Bioinorganic and Materials Chemistry Research Lab. Tribhuvan University, M.M.A.M. Campus, Biratnagar, Nepal.

Publication history**:** Received on 13 July 2020; revised on 19 August 2020; accepted on 21 August 2020

Article DOI: https://doi.org/10.30574/wjarr.2020.8.2.0259

Abstract

This paper deals with the ab initio structure determination of $La_{1.26}\,N_{0.24}\,Na_{2.5}\,O_{2.54}\,Zr_{0.25}$ triclinic structure having triclinic crystal system via powder X-ray data using the Rietveld refinement method, and with physical properties characterization of a related solid solution at the room temperature structure of three compounds belonging to the Aurivillius family $La_{1.26}\,N_{0.24}\,Na_{2.5}\,O_{2.54}\,Zr_{0.25}$ has been analyzed. $La_{1.26}\,N_{0.24}\,Na_{2.5}\,O_{2.54}\,Zr_{0.25}$ crystallizes in a triclinic crystal system with P-1 space group. The starting material was Na_2CO_3,$Zr(NO3)_4$ La2O3 for the Zr,La and Na analogues was derived from ab initio methods and refined using the Rietveld refinement method using JANA software package and visualization by Diamond computer program. The cations Na and La are disordered over the Zr sites while the La cation is found exclusively in the layers. The cell parameters are a=4.1040 Å b=9.9102 Å c=17.6117 Å α=98.4299° β=93.4378° γ=92.2041°.The morphology and electrical properties are carried out of cited oxide.

Keywords: Aurivillius; Rietveld; Ab initio; Triclinic; Structure; Investigation

Graphical Abstract

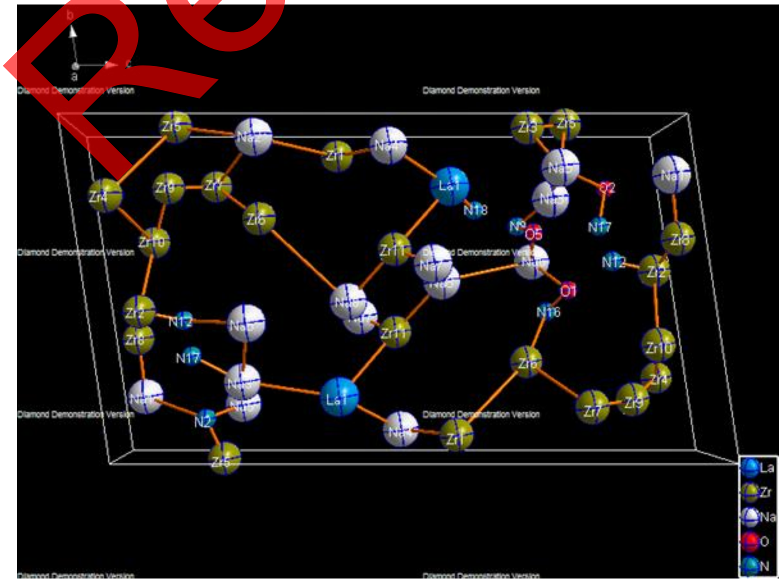

This is 3d dimensional structure of $La_{1.26}\,N_{0.24}\,Na_{2.5}\,O_{2.54}\,Zr_{0.25}$ having triclinic crystal structure obtained via powder X-ray diffraction data and Rietveld refinement by JANA software programme. The cell parameters are a=4.1040 Å b=9.9102 Å c=17.6117 Å α=98.4299° β=93.4378° γ=92.2041°

---

*Corresponding author: Parashuram Mishra

1. Introduction

In materials chemistry, the crystal structure determination is the first step to understand and interpret physical properties of an unknown material. Our understanding of the properties of materials is almost always based on structural information on the atomic scale. Such information is commonly obtained by the wide spread method of X-ray crystallography. However, due to the relatively weak interaction of matter with X-rays, this method is insufficient to investigate extremely small volumes or individual crystals at the scale [1]. Materials with pronounced twinning or new compounds that only exist as part of a complex multi-phase powder sample are thus extremely difficult to treat with this standard method for structure determination. It should be noted that these problem cases also include many technologically relevant products such as small precipitates in a metallic matrix, catalysts, pharmaceuticals, pigments and thin films, which a priori exist only in small quantities or rarely grow as large crystals. Hence, ample motivation exists to develop alternative approaches capable for structural analysis of extremely small volumes and crystallites. However, the only real alternative to X-rays is fast electrons, since their interaction with matter is several orders of magnitude stronger than that of X-rays. Electron diffraction structure analysis (EDSA) makes it, thus, possible to obtain structural information at the atomic level even for the steadily growing number of nanocrystalline materials[2]. On the other hand, structure analysis with electron data is rarely straightforward and fully automated, as it is the case with X-ray data. In particular, the non-kinematical nature of the diffracted intensities is a great concern for structure analysis with electron diffraction data and has hindered EDSA from becoming very popular since its foundation in Russia more than 65 years ago[4]. While a large number of light-atom structures have been investigated by electron diffraction in the past [5], it has only succeeded in a few cases to solve structures with heavier atoms directly from electron diffraction spot patterns. In order to avoid these problems, an alternative approach was developed for such non-light-atom structures. This approach exploits the low-order structure factor phases extracted from high-resolution electron micro microscopy (HREM) images, to assign phases to the higher-order electron diffraction amplitudes [6]. In the most favorite case when the scattering power of the elements in the structure is not too different, the complete structure can be solved from HREM images and subsequently refined with electron diffraction data [7].A recent investigation of structural and conductivity properties of $La_{1.26}$ $N_{0.24}$ $Na_{2.5}$ $O_{2.54}$ $Zr_{0.25}$ oxide conductors (¸La,,Na and Zr), which belong to the triclinic structural-type family, has proved a close conductivity composition dependence [8] This has been interpreted on the basis of structural data obtained from Rietveld structure .The structure is built from cationic slabs parallel to (001) faces of the triclinic cells. There are nine formula units $La_{1.26}$ $N_{0.24}$ $Na_{2.5}$ $O_{2.54}$ $Zr_{0.25}$ triclinic cell, distributed over three slabs. Each slab is constituted from a mixed La3`/¸*n*3` layer, sandwiched between twoLa3` layers[29], and two oxygen sites are located inside; complementary oxide ions, implied by the formulation stoichiometries, are distributed over one or two sites of the inter slab space and exhibit a high mobility, mainly responsible for the conductivity [10].Depending on the rare-earth nature, a b1 high-temperature form is observed, with a closely hexagonal related structure; its formation from the b2 low-temperature variety occurs during a phase transition that has been attributed to a cationic disordering in the mixed Bi3`/¸*n*3` layers. It is accompanied by sudden increases of both lattice parameters, of oxide occupancy in inter slab spaces, and of the conductivity. The pure ion oxide conductor character of the b1 variety has been clearly demonstrated for the alkaline-earth-based solid solutions [11], and has been also verified for lanthanides-based solid solutions. This paper deals with the ab initio structure determination of this new phase from powder X–ray diffraction data and morphology with electrical properties as well.

2. Material and methods

All of the chemical reagents were analytical grade. Na_2SO_4, $Zr(NO_3)_4$ and La_2O_3 were used as starting materials as purchased from Sigma Aldrich with no further purification. The mixture was ground carefully, homogenized thoroughly with methanol (99%) in an agate mortar and then packed into an alumina crucible and calcined at 1000°C in air for 10h with several intermediate grindings [12]. Finally the product was pressed into pallets and sintered at 100 K/h. Powder X-ray diffraction (XRD) data were collected at room temperature in the angular range of$2\theta = 10$ to 90 with scan step width of 0.02° and a fixed containing time of 15 s using Philips powder diffractometer with graphite monochromatic CuKa radiation. The powder was rotated during the data collection to minimize preferred Orientation effect if any. The program TREOR in CRYSFIRE was used to index the powder pattern which give triclinic system.SIRPOW92 was used to locate the positional parameters of constituent atoms. The full pattern is fitting and peak decomposition in the space group P-1 using check cell program. The structural parameters were refined by the Reitveld method using the JANA program which gave Rwp = 0.0317, Rp= 0.022, Rp = 0.052. The density is determined by Archimedes principle. The morphology of titled compound was determined using AFM (Nanoscope III, Digital Instruments, Santa Barbara) For the electrical studies, the measurements were preceded by a pretreatment of the sample in order to reduce the mean particle size 80nm of the obtained powder .After these treatments, the sample achieved about 85% of the theoretical density with the final diameter of 8 mm and thickness of 2 mm. The relative density of the sample before the mechanical grinding was 79 %. Platinum electrodes were connected to the two faces of the pellet via a platinum paste to keep good electric contacts. Impedance spectroscopy measurements were carried out using a Hewlett-Packard 4192a Impedance Analyzer. The impedance spectra were recorded in the 5 Hz-13 MHz frequency range. Electrical conductivity measurements of representative $La_{1.26}N_{0.24}Na_{2.5}O_{2.54}Zr_{0.25}$ were carried out by complex impedance spectroscopy with 1174 Solartron frequency response analyzer coupled to a 1286 Solartron electrochemical interface. Pellets of about 14 mm diameter and 1 mm thickness were prepared by cold pressing of a mechanically activated powder mixture with the composition: $La_{1.26}N_{0.24}Na_{2.5}O_{2.54}Zr_{0.25}$ .To form the phase, the pellets were heated at 700^{0}C during 12 h and slowly cooled to room temperature. This synthesis method was employed to improve the ceramic quality, as it has been shown for other materials [7]. The formed phases and crystallinity were studied by X-ray powder diffraction. Platinum electrodes were deposited on the two faces by sputtering, and measurements were carried out in the temperature range 200-650^{0}C, at steady temperatures, with pellets under air flow. The frequency range was fixed.

3. Results and discussion

In materials chemistry, the crystal structure determination is the first step to understand and interpret physical properties of an unknown material. Moreover, it also guides people on how to modify the material and hence improve the performance [13]. Nowadays, the most successful technique for structure determination is through single crystal X-ray diffraction, from which a sufficient number of independent reflections against the structural parameters can be extracted in 3D reciprocal space. Several mature analysis methods, such as the direct method,1 Patterson method,2 charge-flipping algorithm3 and maximum entropy method4 can be applied to accurately solve the structure. This technique requires synthesizing a high quality single crystal at a micrometer. Experimentally, the chance to get polycrystalline materials is generally larger than to get single crystals. In this case, powder X-ray diffraction (PXRD) becomes a popular technique but with this technique, the possibility to determine an unknown structure dramatically decreases, because 3D reflections are compressed into 1D with an inevitable overlapping problem, especially when the unit cell is big. The situation will become worse when the PXRD is collected on a multi-phase sample, which is not uncommon in the preliminary stage of searching new materials, especially in the cases of hydrothermal (or solvothermal) syntheses of zeolitic or MOF materials'XRD data for the sample of $La_{1.26}N_{0.24}Na_{2.5}O_{2.54}Zr_{0.25}$synthesized at its nominal composition is shown in Figure 1. All peaks could be indexed to a triclinic unit cell with *P-1* symmetry, analogous to the $La_{1.26}N_{0.24}Na_{2.5}O_{2.54}Zr_{0.25}$structure using CRYSFIRE PACKAGE11]. In the diffraction pattern there is a slight anisotropic peak broadening moving to higher angles. This slight peak broadening could be caused by ordering within the cationic layers but relative disorder of the cations between layers. The sloping background observed in XRD at low angles out to ~30° 2θ is qualitatively indicative of stacking faults, a common feature of honeycomb oxides. In an ideal layered mixed-metal oxide, all the cationic planes are stacked along the c-axis by a unique translational stacking vector. However it has been shown that two other stacking vectors with very similar energy (1-2 meV) can occur in a structure, leading to so called "stacking faults". Stacking faults in the honeycomb oxides occur due to the relatively weak coupling between the layers. In practice, the cationic layers are never perfectly stacked along the c-axis when a layered structure has the *P*-1space group, although higher temperature thermal treatment during synthesis can decrease the frequency of stacking faults [8].

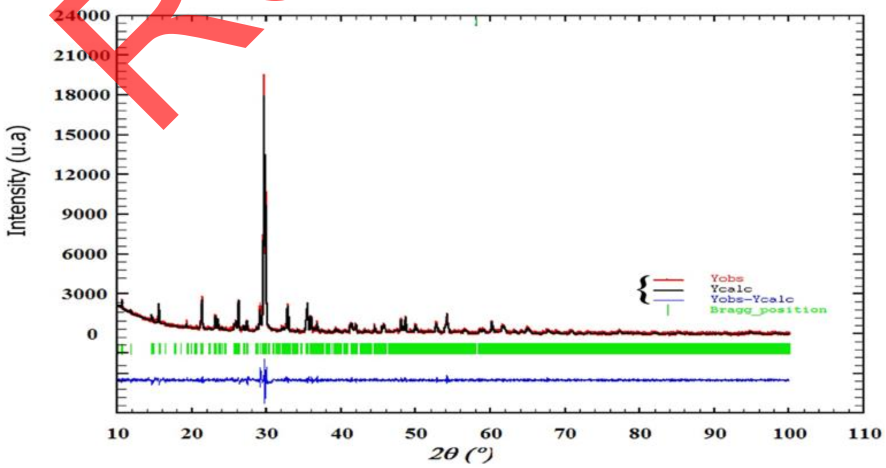

Figure 1 Rietveld refinement of powder $\mathbf{La_{1.26}N_{0.24}Na_{2.5}O_{2.54}Zr_{0.25}}$

Rietveld refinement of Triclinic with P-1 space group $\mathbf{La_{1.26}\ N_{0.24}\ Na_{2.5}\ O_{2.54}\ Zr_{0.25}}$ against XRD data for structural determination proved difficult, due to a combination of preferred orientation of the plate-like crystallites in flat-plate geometry shown in figure 1[14].In other words, the extracted peak intensities for phase 1 could be reliable. Note that if the relative intensities differed a lot from the simulated patterns of the known phases, additional manual partitioning of those overlapping peaks would be necessary to get reliable intensities for the unknown phase 1. After considering the multiplicity and Lorentz-polarization correction, the intensities of phase 1 were used for the structure solution as below. Moreover, the reflection conditions indicated possible space groups P-1 . The initial structure model was obtained using a charge flipping algorithm with the program Superflip.8 [15] The crystallographic data shown in table with triclinic crystal system. Random phases were used at the beginning of the charge-flipping iteration, and overlapping peaks were re-partitioned using a histogram match to improve the convergence. The iteration converged with an R factor of 29% and the final electron density shows aP-1 symmetry with a 5% error. The program of EDMA was then used to automatically assign atomic positions. Four unique heavy atomic positions were found and the heaviest one was assigned as Zr while the others were considered as Zr and La .Due to the existence of heavy atoms, all oxygen positions were ambiguous in the electron density map of this stage[16]. To locate the oxygen and N atoms, a Monte-Carlo based simulated annealing process with the program TOPAS was applied.

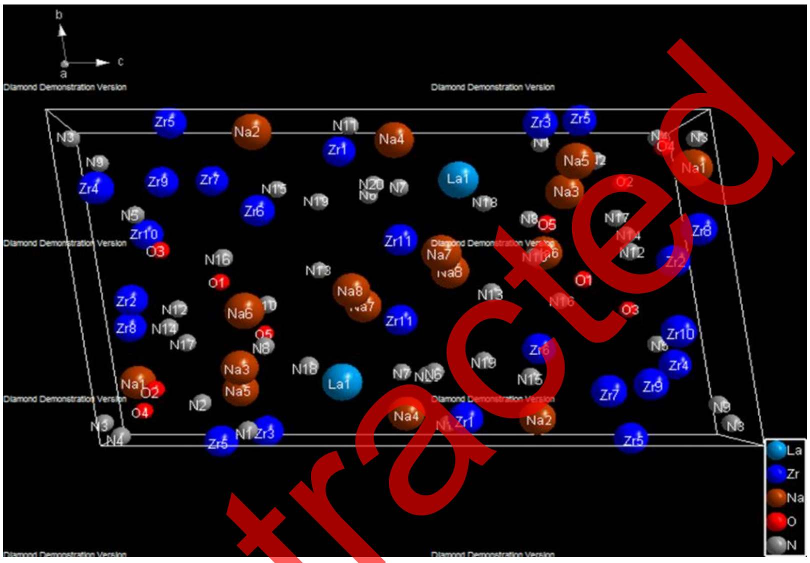

Figure 2 Representation of the Aurivillius type crystal structures of La1.26 N0.24 Na2.5 O2.54 Zr0.25

Table 1 Crystallgraphic Data

Phase data	
Formula sum	$La_{1.26}\ N_{0.24}\ Na_{2.5}\ O_{2.54}\ Zr_{0.25}$
Formula weight	299.3 g/mol
Crystal system	triclinic
Space-group	P -1 (2)
Cell parameters	a=4.1040 Å b=9.9102 Å c=17.6117 Å α=98.4299° β=93.4378° γ=92.2041°
Cell ratio	a/b=0.4141 b/c=0.5627 c/a=4.2913
Cell volume	706.47 $Å^3$
Z	2
Calc. density	1.40691 g/cm^3
Meas. density	1.41231g/cm^3
Pearson code	aP90
Formula type	NO5P8Q11R20
Wyckoff sequence	i45
Indexes	-1≤ h≤,0,0≤,k≤ 2,-1≤,l≤,0

Table 2 Atomic parameters

Atom	Ox.	Wyck.	Site	S.O.F.	x/a	y/b	z/c	U [Å^2]
La1	+3	2i	1		0.47888	0.18164	0.38074	0.0380
Zr1	+4	2i	1		0.77387	-0.07525	0.43773	0.0380
Zr2	+4	2i	1		0.55858	0.43951	0.06303	0.0380
Zr3	+4	2i	1		0.70297	0.02012	0.24521	0.0380
Zr4	+4	2i	1		1.04294	-0.23242	0.05462	0.0380
Zr5	+4	2i	1		0.49036	-0.00441	0.17238	0.0380
Zr6	+4	2i	1		0.36057	-0.28578	0.29122	0.0380
Zr7	+4	2i	1		0.95004	-0.16112	0.21805	0.0380
Zr8	+4	2i	1		0.93594	0.35522	0.04100	0.0380
Zr9	+4	2i	1		0.71646	-0.17787	0.13919	0.0380
Zr10	+4	2i	1		0.90727	-0.33985	0.09533	0.0380
Zr11	+2	2i	1		0.66071	0.37735	0.49238	0.0380
Na1	+1	2i	1		0.96202	0.17267	0.03807	0.0380
Na2	+1	2i	1		0.14511	-0.05766	0.30375	0.0380
Na3	+1	2i	1		0.59234	0.22495	0.21935	0.0380
Na4	+1	2i	1		0.75459	0.07546	0.47844	0.0380
Na5	+1	2i	1		0.90291	0.14934	0.20984	0.0380
Na6	+1	2i	1		0.12986	0.40162	0.24809	0.0380
Na7	+1	2i	1		0.91986	0.42624	0.43763	0.0380
Na8	+1	2i	1		0.53544	0.46951	0.41932	0.0380
O1	-2	2i	1		0.56499	0.49733	0.21132	0.0380
O2	-2	2i	1		0.03295	0.16702	0.09481	0.0380
O3	-2	2i	1		0.25657	-0.41209	0.13068	0.0380
O4	-2	2i	1		0.61082	0.08778	0.05296	0.0380
O5	-2	2i	1		0.83436	0.33490	0.26684	0.0380
N1	-3	2i	1		0.11285	0.04264	0.22398	0.0380
N2	-3	2i	1		0.42074	0.11756	0.15319	0.0380
N3	-3	2i	1		0.48699	0.05238	-0.00961	0.0380
N4	-3	2i	1		0.11562	0.02407	0.02834	0.0380
N5	-3	2i	1		0.34100	-0.30026	0.09808	0.0380
N6	-3	2i	1		0.20558	0.21742	0.52489	0.0380
N7	-3	2i	1		0.58286	0.21147	0.47953	0.0380
N8	-3	2i	1		0.24579	0.29503	0.26899	0.0380
N9	-3	2i	1		0.74344	-0.11621	0.04111	0.0380
N10 -3		2i	1		0.50133	0.42554	0.28131	0.0380

N11 -3	2i	1	0.85231	0.03961	0.54613	0.0380
N12 -3	2i	1	0.63404	0.41283	0.13416	0.0380
N13 -3	2i	1	0.98697	0.54452	0.37316	0.0380
N14 -3	2i	1	0.38902	0.35252	0.12130	0.0380
N15 -3	2i	1	0.71464	-0.20135	0.32517	0.0380
N16 -3	2i	1	0.01663	0.55778	0.22996	0.0380
N17 -3	2i	1	0.52389	0.30466	0.14170	0.0380
N18 -3	2i	1	0.07323	0.23665	0.33308	0.0380
N19 -3	2i	1	0.55976	-0.24902	0.38979	0.0380
N20 -3	2i	1	0.58156	0.20253	0.51923	0.0380

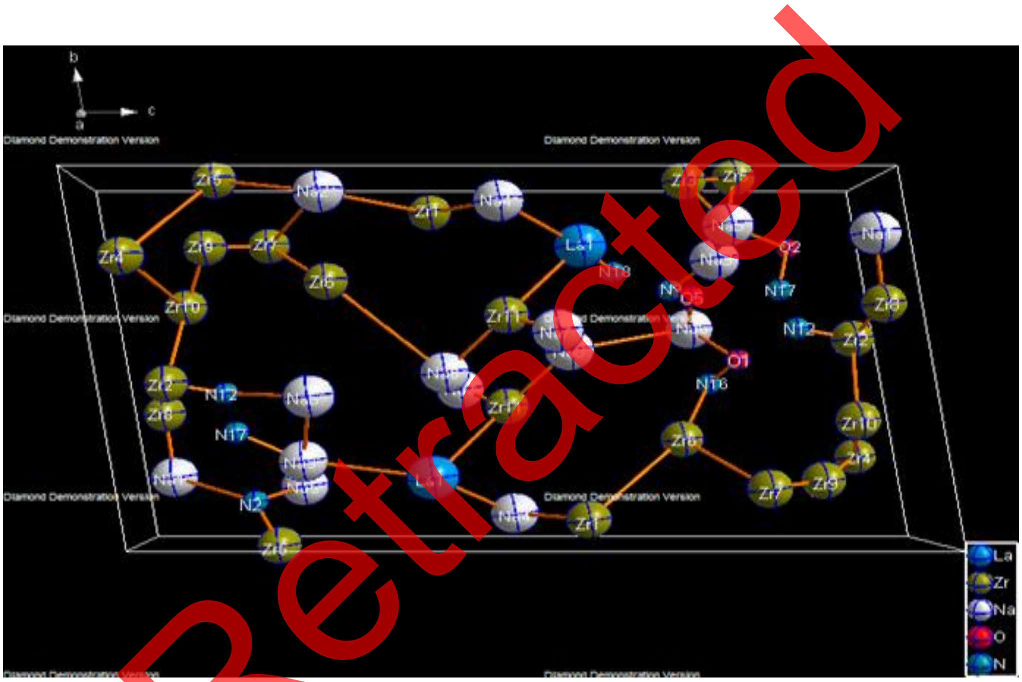

Figure 3 Elliptical 3dimension structure of $La_{1.26} N_{0.24} Na_{2.5} O_{2.54} Zr_{0.25}$

3.1. Crystal Structure of $La_{1.26} N_{0.24} Na_{2.5} O_{2.54} Zr_{0.25}$

The framework structure of $La_{1.26} N_{0.24} Na_{2.5} O_{2.54} Zr_{0.25}$was first examined by ab initio structure determination method using the powder XRD data. The initial lattice parameters were determined to be parameters a=4.1040 Å b=9.9102 Å c=17.6117 Å α=98.4299° β=93.4378° γ=92.2041 and 706.47 Å^{3}by an indexing procedure using the program TREOR15 in EXPO2004. The most probable space group was suggested to be P-1 triclinic crystal system Next, the integrated intensities were extracted by the Le Bail method using the program Jana2006.14 A profile function and background function of the Le Bail method used in the present study were pseudo-Voigt function and 20thorder Legendre function[, respectively. An initial structure model was then obtained by the charge flipping (CF) method17 using the extracted integrated intensities. Although the Zr site could not be clearly determined by the CF method using the powder XRD data, the framework structure of$La_{1.26} N_{0.24} Na_{2.5} O_{2.54} Zr_{0.25}$was successfully determined with the help of Rietveld refinement [17]. Rietveld refinement of Triclinic crystal system having P-1 space group was found with three dimension structure as follows against XRD data for structural determination proved difficult, due to a combination of preferred orientation of the plate-like crystallites in flat-plate geometry. In other words, the extracted peak intensities for phase 1 could be reliable. Note that if the relative intensities differed a lot from the simulated patterns of the known phases, additional manual partitioning of those overlapping peaks would be necessary to get reliable intensities for the unknown phase 1. After considering the multiplicity and Lorentz-polarization correction, the intensities of phase 1 were used for the structure solution as below. Moreover, the reflection conditions indicated possible space groups P-1. The initial structure model was obtained using a charge flipping algorithm with the program Superflip.8. The proper fraction atomic coordinate is giv en in table 2 which are the given positions of contained atoms in the cited oxide. Random phases were used at the beginning of the charge-flipping iteration, and overlapping peaks were re-partitioned using a histogram match to improve the convergence. The iteration converged with an R factor of 29% and the final electron density shows P1 symmetry with a 5% error. The program of EDMA was then used to automatically assign atomic positions. Four unique heavy atomic positions were found and the heaviest one was assigned as Bi while the others were considered as Zr and La. Due to the existence of heavy atoms, all oxygen positions were ambiguous in the electron density map of this stage[18]. To locate the oxygen atoms with metals, a Monte-Carlo based simulated annealing process with the program TOPAS was applied. For each annealing process, various atomic coordinates were randomly assigned as the initial positions of the oxygen atoms [15]. The annealing process was restarted after finding a few oxygen positions, until all oxygen and Nitrogen positions were found to be reasonable. In the structure La is coordinated by trigonal planar geometry with O atoms and Na is also coordinated with N by octahedral along with N and Zr is coordinated with tetrahedral with N atoms.

3.2. AFM investigation of $La_{1.26} N_{0.24} Na_{2.5} O_{2.54} Zr_{0.25}$compound

Topography of $La_{1.26} N_{0.24} Na_{2.5} O_{2.54} Zr_{0.25}$was carried out by AFMtechnique. It was prepared by the hydrothermal air oxidation crystallization method on a large scale (5.6×5.6 µm) is shown ion Fig. 3a, which gives the morphology of titled compound powder in a large area. The image was golden scale – encoded. That is darker regions are deeper than lighter ones and same brightness corresponding to the lights ones is not homogeneous and some powder aggregated lightly. Further information can be obtained from figure 4. (200×200 nm), which shows the size and microstructure of $La_{1.26} N_{0.24} Na_{2.5} O_{2.54} Zr_{0.25}$.aggregates. The size of the aggregates is neither the range of 2.23 nm and the shapes of the aggregates are irregular [19]. A typical image of sample powders, which are prepared by supercritical fluid drying, is shown in Fig. 3b (1.2×1.2 µm image). Some cone like and special particles can be seen individually in the image; the diameters of the particles is roughly 200 nm ~200 nm. It should be noted here that in imaging, rotation of the scan direction and changes of the scan frequency did not affect the structure of $La_{1.26} N_{0.24} Na_{2.5} O_{2.54} Zr_{0.25}$particles, ruling out the possibility that scanning influenced the shapes of these particles or caused some imaging artifact. Moreover, we also found clusters of $La_{1.26} N_{0.24} Na_{2.5} O_{2.54} Zr_{0.25}$particles.in figure 4. The three-dimensional figure can be seen in figure4. .The histogram (volume, area, perimeter vs. Z(nm)) of the desired compound $La_{1.26} N_{0.24} Na_{2.5} O_{2.54} Zr_{0.25}$has been discussed in figure.

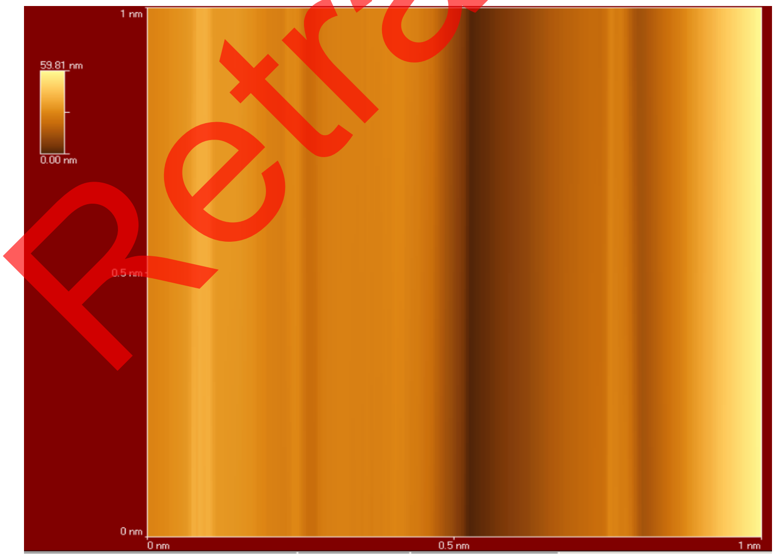

Figure 4 1 ×1 nm AFM picture showing a rather uniform step bunching (not typical)

3.3. Dielectric constant

The dielectric constant and the dielectric loss of the 10 mm in diameter pellet have been used for the determination of dielectric properties of $La_{1.26} N_{0.24} Na_{2.5} O_{2.54} Zr_{0.25}$.The corresponding thickness of the pellet was 1.20 mm was studied at different temperature using a HIOKI 3532-50 LCR HITESTER in the frequency range of 50 Hz to 5 MHz. The results of the dielectric constant and dielectric loss as a function of frequency have been plotted in Figure. It can be easily interpreted from the plots that the $La_{1.26} N_{0.24} Na_{2.5} O_{2.54} Zr_{0.25}$. show same trend, as having high values of dielectric constant and dielectric loss at low frequencies and decrease with the increase in frequency while reaching to a constant saturated value at high frequencies, depicting a frequency independent behavior. These defects activate interfacial polarizations at low frequencies. Due to this polarization, the dielectric constant is higher at low frequencies. The net polarization of silver oxide is owing to ionic, electronic, dipolar and space charge polarizations [19]. The huge value of the dielectric constant is due to the fact that silver oxide acts as a nano dipole under electric fields. The small-sized particles require a large number of particles per unit volume, important in an increase of the dipole moment per unit volume, and a high dielectric constant. The dielectric constant at low frequencies starts from high value and decreases with increase in temperature. As the temperature increases, the dielectric constant values start increasing. The high value of dielectric constant at low temperature credited to space charge polarization whereas at higher temperature and at low frequencies it possibly connected with defect related conduction processes [21]. The variations of dielectric loss of $La_{1.26}N_{0.24}Na_{2.5}O_{2.54}Zr_{0.25}$.of with frequency and temperature are shown in Figure [5]. It can be seen that dielectric loss decreases with increase of frequency and at higher frequencies the loss angle has almost the same value at all temperatures. In dielectric materials, generally dielectric losses take place due to absorption current. The orientation of molecules along the direction of the applied electric field in polar dielectrics requires a part of electric energy to overcome the forces of internal friction. One more part of electric energy is utilized for rotations of dipolar molecules and other kinds of molecular transfer from one position to another, which also involve energy losses. In nanophase materials, in homogeneities similar to defects and space charge formation in the inter phase layers create an absorption current ensuing in a dielectric loss.

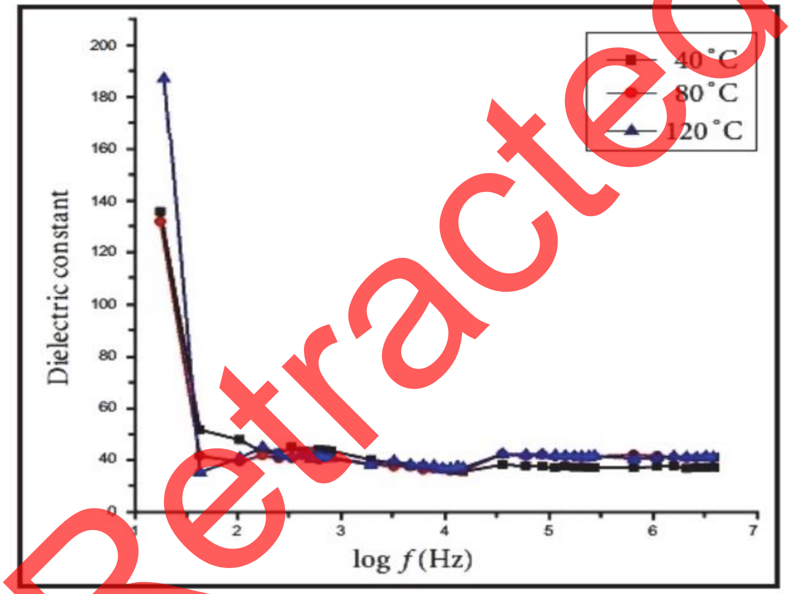

Figure 5 Dielectric constant as a function of log frequency

The titled metal oxide show nanopartice according to particle size determine with help of fulwidth half maxima [FWHM] 100% intensity which are placed in the heater and their response is taken at different temperatures. Temperature dependent dielectric constant and dielectric loss. It is also observed that as the temperature increases, the dielectric constant also increases to a considerable value as seen in Figure. The same trend is observed behavior of dielectric properties with temperature is different over different temperature ranges i.e. at low and high temperature. It is evident that the dielectric constant and dielectric loss are low at a certain room temperature range and remain independent of temperature changes. In high temperature range the dielectric properties rise suddenly and reach a maximum value. The basic reason of the independency of dielectric constant in low temperature range is that impurities remain localized in this range and so conduction is not easy while at high temperature impurities are no more localized and hence conductivity of the material is increased. In case of ionic solids, electrons of the material also become free and contribute to conduction. This results in high polarization of the material; hence value of dielectric constant is increased with increase in temperature. At low and room temperature range, the effect of grain boundaries is dominant and that is why the dielectric properties have small magnitudes and are constant. As the temperature is increased, the role of grains becomes more and more effective and increases in the dielectric properties [22].

4. Conclusion

The titled metal oxide show nanopartice according to particle size determine with help of fulwidth half maxima [FWHM] 100% intensity which are placed in the heater and their response is taken at different temperatures. Temperature dependent dielectric constant and dielectric loss. It is also observed that as the temperature increases, the dielectric constant also increases to a considerable value as seen in Figure . The same trend is observed behavior of dielectric properties with temperature is different over different temperature ranges i.e. at low and high temperature. It is evident that the dielectric constant and dielectric loss are low at a certain room temperature range and remain independent of temperature changes. In high temperature range the dielectric properties rise suddenly and reach a maximum value. The basic reason of the independency of dielectric constant in low temperature range is that impurities remain localized in this range and so conduction is not easy while at high temperature impurities are no more localized and hence conductivity of the material is increased. In case of ionic solids, electrons of the material also become free and contribute to conduction. This results in high polarization of the material; hence value of dielectric constant is increased with increase in temperature. At low and room temperature range, the effect of grain boundaries is dominant and that is why the dielectric properties have small magnitudes and are constant. As the temperature is increased, the role of grains becomes more and more effective and increases in the dielectric properties.

Compliance with ethical standards

Acknowledgments

The authors would like to acknowledge the immense contribution laboratory staff of Department of Chemistry University of Delhi, India for provide the XRD data.

Disclosure of conflict of interest

The authors declare that they have no conflict of interest.

References

[1] Parveen R, Dharam PS and Parveen S. (2015). Synthesis, characterization, powder XRD and antimicrobial-antioxidant activity evaluation of trivalent transition metal macrocyclic complexes, C. R. Chimie, 18,430–437.

[2] Kai Li and Rik VD. (2019). Novel Intense Emission-Tunable Li1.5La1.5WO6:Mn4+,Nd3+,Yb3+Material with Good Luminescence Thermal Stability for Potential Applications in Si Solar Cells and Plant-Cultivation Far-Red-NIR LEDs, ACS Sustainable Chem. Eng, 7, 16284–16294.

[3] Peng Q, Cao R, Ye YG, S Hu, Z Chen and T Zheng G. (2017). Photoluminescence properties of broadband deep-red-emitting Na2MgAl10O17:Mn4+ phosphor. J. Alloys Compd, 725, 139–144.

[4] J You, L Xin, X Yu, X Zhou and Y Liu. (2018). Synthesis ofhomogenous CaMoO4 microspheres with nanopits forhigh-caapcity anode material in Li-ion battery, Appl. Phys.A: Mater. Sci. Process, 124, 271- 580.

[5] Y Liang, X Han, Z Yi, W Tang, L Zhou, J Sun, S Yang and Y Zhou. (2017). Synthesis, characterization and lithium intercalation properties of rod-like CaMoO4 nanocrystals,J. Solid State Electrochem, 11, 1127–1131.

[6] Parashuram M. (2011). Synthesis, crystal structure determination and ionic properties of novel BiCa0.5Mg0.5 O2.5 via X- ray powder diffraction data Crystal Growth, 2041(32), 2041-204.

[7] Philipp B, Christoph B, Bruno ACB and Carsten J. Marc C. Nierstenhöfer1 Journal of Chemical Crystallography.

[8] Mah J, Abdessalem B and Mongi BA. Journal of Chemical Crystallography.

[9] N Tancret, S Obbade, N Bettahar and F Abraha. (1996). journal of solid state chemistry, 124, 309–318.

[10] T Dan Vu, FirasK, Maud B, Sandrine C, Alain Jouanneaux,† Emmanuelle Suard,§Andrew Fitch,‖ and FrançoisGoutenoire(2012) . Ab initio structure determination of mixe valence oxide,, J .of solid State Chemistry132,4,152-160.

[11] Florian P, Massiot D, Suard E and Goutenoire F. (2014). La10W2O21: An Anion-Deficient Fluorite-Related Superstructure with Oxide Ion Conduction. Inorg. Chem. 53, 147–159.

[12] Lopez-Vergara A, Porras-Vazquez JM, Infantes-Molina A, Canales -Vazquez J, Cabeza A, Losilla ER and Marero-Lopez D. (2017). Effect of Preparation Conditions on the Polymorphism and Transport Properties of La6−xMoO12−δ (0 ≤ x ≤ 0.8). Chem. Mater, 29, 6966–6975.

[13] Dubois F, Goutenoire F, Laligant Y, Suard E and Lacorre P. (2001). Ab-Initio Determination of La2Mo4O15 Crystal Structure from X-rays and Neutron Powder Diffraction. J. Solid State Chem, 159, 228–233.

[14] Thomas EW,Joaquim P, Gerhard C,Hartmut H and Stavros N. (2006). Ab initio determination of the framework structure of the heavy-metal oxide CsxNb2.54W2.46O14 from 100 kV precession electron diffraction Ultramicroscopy, 106, 164–175.

[15] AP Zhukhlistov, MS Nickolsky, BB Zvyagin, AS Avilov, AK Kulygin, S Nicolopoulos, R Ochs and Z Kristallographie. (2004), Morphology and crystal structure of metal oide contained mixed valence by ab initio methods,J.Ionic Solids, 45 219-. 224.

[16] DO Charkin. (2008). Modular approach as applied to the description, prediction, and targeted synthesis of bismuth oxohalides with layered structures, Russ. J. Inorg. Chem. Suppl, 53, 1977–1996,

[17] G Kresse and D Joubert. (1999).From ultrasoft pseudo potentials to the projector augmented wave method, Phys. Rev, B 59, 1758–1775.

[18] Zhengyang Z, Lukáš P and Junliang S. Structure determination of modulated structures by powder X-ray diffraction and electron diffraction, Inorganic Chemistry Frontiers.

[19] T Dan Vu, Firas K, Maud B, Sandrine C, Alain J, Emmanuelle S, Andrew F and François G. Ab Initio Structure Determination of La34Mo8O75 Using Powder X-ray and Neutron Diffraction Data.

[20] Chambrier MH, Le Bail A, Giovannelli F, Redjaimia A, Florian P, Massiot D, Suard E and Goutenoire F. (2014). La10W2O21: AnAnion-Deficient Fluorite-Related Superstructure with Oxide Ion Conduction. Inorg. Chem, 53, 147–159.

[21] Lopez-Vergara A, Porras-Vazquez JM, Infantes-Molina A, Canales -Vazquez J, Cabeza A, Losilla ER and Marero-Lopez D. (2017). Effect of Preparation Conditions on the Polymorphism and Transport Properties of La6−xMoO12−δ (0 ≤ x ≤ 0.8). Chem. Mater, 29,6966–6975.

[22] Dmitri OC, Andrey SK, Sergey MK, Igor VP, Anastasiya IZ, Alexey NK, Konstantin IM, Anton YT, Yury AT, Alexander NZ and Oleg IS. (2019). Synthesis, crystal structure, spectroscopic properties, and thermal behavior of rare-earth oxide selenates, Ln2O2SeO4 (Ln ¼ La, Pr, Nd): The new perspectives of solid-state double-exchange synthesis, Journal of Solid State Chemistry, 277, 163–168.

[23] Wu L, Bai Y, Wu L, Yi H, Zhang X, Zhang L, Kong Y, Zhang and Y Xu J. (2018). Analysis of the structure and abnormal photoluminescence of a red-emitting LiMgBO3:Mn2+ phosphor. Dalton Trans. 2018, 47, 13094–13105.